

# Post-conjunction detection of $\beta$ Pictoris b with VLT/SPHERE <sup>★</sup>

A.-M. Lagrange<sup>1</sup>, A. Boccaletti<sup>2</sup>, M. Langlois<sup>3,4</sup>, G. Chauvin<sup>1,5</sup>, R. Gratton<sup>6</sup>, H. Beust<sup>1</sup>, S. Desidera<sup>6</sup>, J. Milli<sup>7</sup>, M. Bonnefoy<sup>1</sup>, A. Cheetham<sup>15</sup>, M. Feldt<sup>8</sup>, M. Meyer<sup>9,10</sup>, A. Vigan<sup>3</sup>, B. Biller<sup>8,11</sup>, M. Bonavita<sup>6,11</sup>, J.-L. Baudino<sup>6,12</sup>, F. Cantalloube<sup>8</sup>, M. Cudel<sup>1</sup>, S. Daemgen<sup>9</sup>, P. Delorme<sup>1</sup>, V. D'Orazi<sup>6</sup>, J. Girard<sup>1</sup>, C. Fontanive<sup>6,11</sup>, J. Hagelberg<sup>1</sup>, M. Janson<sup>8,13</sup>, M. Keppler<sup>8</sup>, T. Koypitova<sup>8</sup>, R. Galicher<sup>2</sup>, J. Lannier<sup>1</sup>, H. Le Coroller<sup>3</sup>, R. Ligi<sup>3,20</sup>, A.-L. Maire<sup>8</sup>, D. Mesa<sup>6</sup>, S. Messina<sup>14</sup>, A. Müller<sup>8</sup>, S. Peretti<sup>15</sup>, C. Perrot<sup>2</sup>, D. Rouan<sup>2</sup>, G. Salter<sup>3</sup>, M. Samland<sup>8</sup>, T. Schmidt<sup>2</sup>, E. Sissa<sup>6</sup>, A. Zurlo<sup>3,16</sup>, J.-L. Beuzit<sup>1</sup>, D. Mouillet<sup>1</sup>, C. Dominik<sup>17</sup>, T. Henning<sup>8</sup>, E. Lagadec<sup>18</sup>, F. Ménard<sup>1</sup>, H.-M. Schmid<sup>9</sup>, M. Turatto<sup>6</sup>, S. Udry<sup>15</sup>, A.J. Bohn<sup>19</sup>, B. Charnay<sup>2</sup>, C. A. Gomez Gonzales<sup>1</sup>, C. Gry<sup>3</sup>, M. Kenworthy<sup>19</sup>, Q. Kral<sup>2</sup>, C. Mordasini<sup>22</sup>, C. Moutou<sup>3</sup>, G. van der Plas<sup>19</sup>, J. E. Schlieder<sup>21,15</sup>, L. Abe<sup>18</sup>, J. Antichi<sup>23</sup>, A. Baruffolo<sup>6</sup>, P. Baudoz<sup>2</sup>, J. Baudrand<sup>2</sup>, P. Blanchard<sup>3</sup>, A. Bazzon<sup>9</sup>, T. Buey<sup>2</sup>, M. Carillet<sup>18</sup>, M. Carle<sup>3</sup>, J. Charton<sup>1</sup>, E. Cascone<sup>24</sup>, R. Claudi<sup>6</sup>, A. Costille<sup>3</sup>, A. Deboulbe<sup>1</sup>, V. De Caprio<sup>24</sup>, K. Dohlen<sup>3</sup>, D. Fantinel<sup>6</sup>, P. Feautrier<sup>1</sup>, T. Fusco<sup>25</sup>, P. Gigan<sup>2</sup>, E. Giro<sup>6</sup>, D. Gisler<sup>9</sup>, L. Gluck<sup>1</sup>, N. Hubin<sup>26</sup>, E. Hugot<sup>3</sup>, M. Jaquet<sup>3</sup>, M. Kasper<sup>26</sup>, F. Madec<sup>3</sup>, Y. Magnard<sup>1</sup>, P. Martinez<sup>18</sup>, D. Maurel<sup>1</sup>, D. Le Mignant<sup>3</sup>, O. Möller-Nilsson<sup>8</sup>, M. Llored<sup>3</sup>, T. Moulin<sup>1</sup>, A. Origné<sup>3</sup>, A. Pavlov<sup>8</sup>, D. Perret<sup>2</sup>, C. Petit<sup>25</sup>, J. Pragt<sup>27</sup>, J. Szulagyi<sup>28</sup>, and F. Wildi<sup>15</sup>

(Affiliations can be found after the references)

Received date: this version XXX / Accepted date

## ABSTRACT

**Context.** With an orbital distance comparable to that of Saturn in the solar system,  $\beta$  Pictoris b is the closest (semi-major axis  $\approx 9$  au) exoplanet that has been imaged to orbit a star. Thus it offers unique opportunities for detailed studies of its orbital, physical, and atmospheric properties, and of disk-planet interactions. With the exception of the discovery observations in 2003 with NaCo at the Very Large Telescope (VLT), all following astrometric measurements relative to  $\beta$  Pictoris have been obtained in the southwestern part of the orbit, which severely limits the determination of the planet's orbital parameters.

**Aims.** We aimed at further constraining  $\beta$  Pictoris b orbital properties using more data, and, in particular, data taken in the northeastern part of the orbit.

**Methods.** We used SPHERE at the VLT to precisely monitor the orbital motion of beta  $\beta$  Pictoris b since first light of the instrument in 2014.

**Results.** We were able to monitor the planet until November 2016, when its angular separation became too small (125 mas, i.e., 1.6 au) and prevented further detection. We redetected  $\beta$  Pictoris b on the northeast side of the disk at a separation of 139 mas and a PA of  $30^\circ$  in September 2018. The planetary orbit is now well constrained. With a semi-major axis (sma) of  $a = 9.0 \pm 0.5$  au ( $1\sigma$ ), it definitely excludes previously reported possible long orbital periods, and excludes  $\beta$  Pictoris b as the origin of photometric variations that took place in 1981. We also refine the eccentricity and inclination of the planet. From an instrumental point of view, these data demonstrate that it is possible to detect, if they exist, young massive Jupiters that orbit at less than 2 au from a star that is 20 pc away.

**Conclusions.**

**Key words.** stars: planetary systems – stars: individual:  $\beta$  Pictoris – Techniques: high angular resolution

## 1. Introduction

With its imaged debris disk of dust (see [Smith & Terrile 1984](#), for the discovery image), its falling, evaporating exocomets ([Kiefer et al. 2014](#), and references therein), and an imaged giant planet ([Lagrange et al. 2010](#)), the  $\sim 20$  Myr old  $\beta$  Pictoris is a unique proxy for the study of the early stages of planetary system formation and evolution, when giant planets are formed, Earth-mass planets may still be forming, and most of the protoplanetary gas has disappeared from the disk. Its proximity to Earth ([van Leeuwen 2007](#), distance =  $19.454 \pm 0.05$  pc) and the relatively short ( $\approx$  two decades) orbital period of  $\beta$  Pictoris b enable detailed studies of its orbit and its physical and atmospheric

properties. The system also allows us to study the interaction between planet(s) and disks.  $\beta$  Pictoris b can explain, for example, several (but not all) of the dust disk morphologies, in particular its inner warp, and some outer asymmetries ([Lagrange et al. 2010](#)).  $\beta$  Pictoris b could also be the trigger for the infall and evaporation of cometary bodies (exocomets) onto the star, if it has a non-zero eccentricity ([Beust & Morbidelli 1996](#)). Last,  $\beta$  Pictoris b was suggested to be responsible for the photometric variations observed in 1981 ([Lecavelier Des Etangs et al. 1995](#)) and has tentatively been attributed to a planet transit ([Lecavelier Des Etangs et al. 1997](#)).

Careful monitoring of the position of the planet relative to the star (referred to as astrometric measurements) with the Nasmyth Adaptive Optics System (NAOS) Near-Infrared Imager and Spectrograph (CONICA) (NaCo) at the Very Large Telescope (VLT) constrained its orbital properties ([Bonnefoy et al. 2014a](#); [Chauvin et al. 2012](#)). By combining data from NaCo

Send offprint requests to: Anne-Marie Lagrange, e-mail: anne-marie.lagrange@at.univ-grenoble-alpes.fr

<sup>★</sup> Based on observations collected at the European Southern Observatory under programmes 198.C-0209, 1100.C-0481

and the Gemini Planetary Imager (GPI), Wang et al. (2016) found a similar but slightly different orbit. Assuming that the peculiar photometric event observed in 1981 could be due to the transit of  $\beta$  Pictoris b in front of the star, Lecavelier des Etangs & Vidal-Madjar (2016) identified a second family of orbital solutions: a semi-major axis  $a = 13$  au instead of 9 au, that is, a period of 34 yr instead of about 20 yr, and  $e = 0.3$  instead of less than 0.1. Recently, Snellen & Brown (2018) used GAIA and HIPPARCOS measurements to constrain the planet period to  $\geq 22$  yr, and reported a mass of  $11 \pm 2 M_{\text{Jup}}$ , which is compatible with the constraints derived from radial velocity data alone (Lagrange et al. 2012b) or by the combined analysis of direct imaging and radial velocity data (Bonnetfoy et al. 2014a).

$\beta$  Pictoris b was discovered northeast of the star in data obtained in 2003 with NaCo. All available images in addition to this discovery image were obtained in 2009 and later, as the planet orbited southwest of the star, after it passed behind the star (Lagrange et al. 2010). The orbital plane is close to equatorial, and the disk of  $\beta$  Pictoris is seen almost edge-on. This geometrical configuration prevented following the planet in direct imaging when it was projected too close (typically less than 120 mas) to the star. Altogether, only about 50% of the planetary orbit had been monitored thus far, including the 2003 epoch, which suffers from relatively large uncertainties and thus limits the precision on the orbital parameters of the planet. We here present a homogeneous set of planet observations obtained with the Spectro-Polarimetric High-Contrast Exoplanet Research instrument (SPHERE), and in particular, the recent recovery of the planet in September 2018. The observations are described in Section 2, and the results are shown and discussed in Sections 3.

## 2. Observations

High-contrast coronagraphic SPHERE (Beuzit et al. 2008) observations were obtained between December 2014 and November 2016, and in September 2018, using the IRDIFS mode in the context of the SpHere Infrared survey for Exoplanets (SHINE, Chauvin et al. 2017a). In this setup, the IRDIS (Dohlen et al. 2008) and IFS (Claudi et al. 2008) instruments operate simultaneously. The data were obtained under various atmospheric conditions (see Table 1) with the H2 ( $\lambda_c = 1.593 \mu\text{m}$ ;  $\Delta\lambda = 0.055 \mu\text{m}$ ) and H3 ( $\lambda_c = 1.667 \mu\text{m}$ ;  $\Delta\lambda = 0.056 \mu\text{m}$ ) narrow bands of IRDIS, except in December 2014, when we used the K1 ( $\lambda_c = 2.1025 \mu\text{m}$ ;  $\Delta\lambda = 0.102 \mu\text{m}$ ) and K2 ( $\lambda_c = 2.255 \mu\text{m}$ ;  $\Delta\lambda = 0.109 \mu\text{m}$ ) narrow bands. The IRDIS images have a field of view (FoV) of  $\sim 10'' \times 11''$ , and a pixel size of approximately 12.25 mas. IFS data were also recorded, but they are not analyzed here. We used apodized Lyot coronagraphs that include either a 185 mas diameter focal mask (N\_ALC\_YJH\_S) or, when the planet was closer to the star, a smaller (145 mas) mask (N\_ALC\_YJ\_S), combined to an apodizer as well as a pupil stop (Carillet et al. 2011). All coronagraphic data were recorded in stabilized pupil mode so as to apply angular differential imaging (ADI) post-processing techniques to remove the stellar halo, as described in Marois et al. (2006). Most coronagraphic data were also recorded while four satellite footprints of the point spread function (PSF) had been created by the deformable mirror of the instrument and were used for fine monitoring of the frame centering and for photometric purposes. The FoV rotation during the coronagraphic observations varied between  $16^\circ$  and  $54^\circ$  (see Table 1).

Each observing sequence was obtained with the following pattern: PSF - coronagraphic observations - PSF - sky. The PSF

data correspond to non-saturated exposures of the star placed out of the coronagraphic mask and obtained using a neutral density filter. They are used for relative photometric reference and to estimate the image quality at the beginning and end of the observations. The sky data were recorded at the end of the coronagraphic sequence to estimate the background level and hot pixels in the science images. Finally, an astrometric field, either Orion or 47 Tuc, was observed with IRDIS for each run (see Maire et al. 2016). In the case of Orion, the sub-field we used was chosen to be part of the one considered with NaCo since 2008 to allow the best match between the astrometric calibrations of NaCo and SPHERE. The pixel scales and north positions are provided in Table 1.

The data were reduced as described in Chauvin et al. (2017b) and using the SpeCal tool developed for SPHERE (Galicher et al. 2018).  $\beta$  Pictoris b is clearly detected in all images taken between 2014 and 2016, orbiting SW of the star at signal-to-noise ratio (S/N) higher than 9 (Table 2). Fig. 1 shows images of the planet at various dates, and Table 2 provides the relative position of the planet with respect to the star<sup>1</sup>. The S/N is relatively poor in the last observation of November 2016, as the projected separation of the planet from the star is less than 125 mas ( $\approx 1.5$  au only) and the contrast is about 9.5 mag, which leads to larger error bars on its astrometry. To our knowledge, neither  $\beta$  Pictoris b nor any other planet has ever been imaged at such a close projected separation to the star. The 2018 data clearly reveal the planet at 139 mas NE (P.A. about  $30^\circ$ ) from the star.

## 3. Orbital properties of $\beta$ Pictoris b

With these additional SPHERE data, a large part of the orbit is now sampled, as seen in Fig. 2. We used the positions of the planet relative to the star in these data as well as in the previously published NaCo data (Bonnetfoy et al. 2014a) together with the Markov chain Monte Carlo (MCMC) Bayesian analysis technique described in Chauvin et al. (2012) to derive the probabilistic distribution of the orbital solutions. The results are shown in Fig. 3. For comparison, we show in Fig. 4 the parameters that we deduce with and without the September 2018 data to illustrate the importance of this post-conjunction detection for constraining the orbital properties of the planet.

From Fig. 4, we derive the following  $1\sigma$  confidence intervals for the major orbital parameters:  $a = 8.90^{+0.25}_{-0.41}$  au for the semi-major axis,  $P = 20.29^{+0.86}_{-1.35}$  yr for the orbital period,  $e = 0.01^{+0.029}_{-0.01}$  for the eccentricity, and  $i = 89.08^{+0.16}_{-0.19}$  for the inclination. We note that the orbital period distribution is compatible with a period greater than 22 yr found by Snellen & Brown (2018) within only  $2\sigma$  error bars.

The sma found is compatible with the value derived by Bonnetfoy et al. (2014a), and definitely excludes the long-period solution proposed by Lecavelier des Etangs & Vidal-Madjar (2016) that assumed a transit of the planet in 1981. Snellen & Brown (2018) predicted a period longer than 22 yr, while the period we derive here is rather 20 yr. We note, however, that the result from the Snellen & Brown (2018) relies on the assumption that there is only one planet around  $\beta$  Pictoris, which is not

<sup>1</sup> The planet was hardly or even not at all detected in November 2016 with the TLOCI algorithm (Marois et al. 2014), while it was detected using a principal component analysis (PCA Soummer et al. (2012)) algorithm. For consistency, all position measurements were obtained on PCA images.

**Table 1.** Observing log

Date UT (yyyy-mm-dd)	Filters	DIT×NDIT×Nexp (s)	AM	$\Delta$ par ( $^{\circ}$ )	DIMM seeing ( $''$ )	$\tau_0$ (ms)	TNcorr ( $^{\circ}$ )	Plate scale (mas/pix)
2014-12-08	IRDIS-K1K2	4×40×36	1.12	16.4	0.75	4.4	-1.71	12.251
2015-02-05	IRDIS-H2H3	4×40×8	1.16	43.0	0.78	7.8	-1.72	12.255
2015-10-01	IRDIS-H2H3	4×16×2	1.15	22.8	1.42	1.0	-1.81	12.250
2015-11-30	IRDIS-H2H3	4×80×32	1.12	39.9	1.06	10.1	-1.75	12.255
2015-12-26	IRDIS-H2H3	8×98×20	1.12	36.6	1.44	2.1	-1.79	12.255
2016-01-20	IRDIS-H2H3	4×60×30	1.12	29.3	0.60	3.0	-1.81	12.255
2016-03-27	IRDIS-H2H3	8×20×32	1.28	19.9	0.74	1.7	-1.77	12.255
2016-04-16	IRDIS-H2H3	8×42×32	1.42	17.9	0.65	6.0	-1.74	12.255
2016-09-16	IRDIS-H2H3	8×16×8	1.17	38.6	0.32	1.2	-1.76	12.255
2016-10-14	IRDIS-H2H3	16×8×10	1.12	53.8	0.75	3.0	-1.76	12.255
2016-11-18	IRDIS-H2H3	2×64×50	1.12	39.8	0.96	2.0	-1.76	12.248
2018-09-17	IRDIS-H2H3	2×30×46	1.17	36.6	0.69	3.7	-1.79	12.239

**Notes.** AM stands for the mean airmass,  $\Delta$ par for the variation in parallactic angle during the coronagraphic sequence, TNcorr for true north correction (TN is the angle between the north position and the detector "North"). Seeing and coherence time ( $\tau_0$ ) are mean values throughout the coronagraphic sequence.

**Table 2.** Relative astrometry of  $\beta$  Pictoris b

Date UT	separation (mas)	PA ( $^{\circ}$ )	S/N
2014-12-08	350.51 ± 3.20	212.60 ± 0.66	62
2015-02-05	332.42 ± 1.70	212.58 ± 0.35	63
2015-10-01	262.02 ± 1.78	213.02 ± 0.48	41
2015-11-30	242.05 ± 2.51	213.30 ± 0.74	40
2015-12-26	234.84 ± 1.80	213.79 ± 0.51	41
2016-01-20	227.23 ± 1.55	213.15 ± 0.46	62
2016-03-26	203.66 ± 1.42	213.90 ± 0.46	68
2016-04-16	197.49 ± 2.36	213.88 ± 0.83	34
2016-09-16	142.36 ± 2.34	214.62 ± 1.10	18
2016-10-14	134.50 ± 2.46	215.50 ± 1.22	27
2016-11-18	127.12 ± 6.44	215.80 ± 3.37	10
2018-09-17	140.46 ± 3.12	29.71 ± 1.67	19

necessarily correct. Finally, based on our values, the 2017 conjunction took place in  $2017.72 \pm 0.04$ , and the next conjunction will occur in 2038.06.

The orbital solution favors a very low eccentricity but still remains compatible with zero. We note that the peak of the distribution is now slightly off zero, in contrast with previous determinations (Bonnefoy et al. 2014b). Previous studies (Beust & Morbidelli (1996), Beust & Morbidelli (2000) and Thébault & Beust (2001)) of the falling evaporating bodies scenario showed that this phenomenon could be explained by the perturbing action of a giant planet orbiting at  $\sim 10$  au from the star, if it has a low orbital eccentricity.  $\beta$  Pictoris b might of course be assimilated to this planet, and the fact that its eccentricity might be non-zero is a key point for this scenario.

Finally, the large FoV of IRDIS enables detecting the disk and the planet in the same image. The SPHERE data confirm the conclusions reached in Lagrange et al. (2012a): the planet projection is between the main disk and the warp.

#### 4. Concluding remarks and perspectives

The sensitivity of SPHERE allowed us to follow  $\beta$  Pictoris b down to 125 mas from the star in projected separation. The latest measurements reveal the planet on the NE side of the star, for

the first time since its discovery. It was last detected in November 2016 and was redetected in September 2018. Based on the observed data, the semi-major axis of the planet is well constrained to  $8.90^{+0.25}_{-0.41}$  au ( $1 \sigma$ ), its eccentricity to  $e = 0.01^{+0.029}_{-0.01}$ , and its inclination to  $89.08^{+0.16}_{-0.19}$  degrees. The data do not support that the planet was responsible for the photometric event in 1981. More data obtained in the NE part of the disk will allow further refining the orbital properties of the planet. Further work will include the combination of these new, crucial astrometric data points with our latest radial velocity measurements and, if possible, a combination with GAIA and HIPPARCOS data to constrain the dynamical mass of the planet. From an instrumental point of view, these data demonstrate that if they exist, SPHERE can detect young and massive Jupiters as close as 1.6 au from a star located at 20 pc.

*Acknowledgements.* We acknowledge financial support from the Programme National de Planétologie (PNP) and the Programme National de Physique Stellaire (PNPS) of CNRS-INSU. This work has also been supported by a grant from the French Labex OSUG@2020 (Investissements d'avenir ANR10 LABX56). The project is supported by CNRS, by the Agence Nationale de la Recherche (ANR-14-CE33-0018). This work has made use of the the SPHERE Data Centre, jointly operated by OSUG/IPAG (Grenoble), PYTHEAS/LAM/CESAM (Marseille), OCA/Lagrange (Nice) and Observatoire de Paris/LESIA (Paris). AML thanks Julian Mejia for his help during the September 2018 DVM observations, Nadège Meunier, Eric Lagadec, and Philippe Delorme for their assistance in the DC process, and Pascal Rubini for his help in the scheduling of the observations. E.S., R.G., D.M., S.D. and R.U.C. acknowledge support from the "Progetti Premiali" funding scheme of the Italian Ministry of Education, University, and Research. SPHERE is an instrument designed and built by a consortium consisting of IPAG (Grenoble, France), MPIA (Heidelberg, Germany), LAM (Marseille, France), LESIA (Paris, France), Laboratoire Lagrange (Nice, France), INAF Osservatorio Astronomico di Padova (Italy), Observatoire de Genève (Switzerland), ETH Zurich (Switzerland), NOVA (Netherlands), ONERA (France) and ASTRON (Netherlands) in collaboration with ESO. SPHERE was funded by ESO, with additional contributions from CNRS (France), MPIA (Germany), INAF (Italy), FINES (Switzerland) and NOVA (Netherlands). SPHERE also received funding from the European Commission Sixth and Seventh Framework Programmes as part of the Optical Infrared Coordination Network for Astronomy (OPTICON) under grant number RII3-Ct-2004-001566 for FP6 (2004-2008), grant number 226604 for FP7 (2009-2012) and grant number 312430 for FP7 (2013-2016).

#### References

- Beust, H. & Morbidelli, A. 1996, *Icarus*, 120, 358  
 Beust, H. & Morbidelli, A. 2000, *Icarus*, 143, 170

- Beuzit, J.-L., Feldt, M., Dohlen, K., et al. 2008, in Society of Photo-Optical Instrumentation Engineers (SPIE) Conference Series, Vol. 7014
- Bonnefoy, M., Marleau, G.-D., Galicher, R., et al. 2014a, *A&A*, 567, L9
- Bonnefoy, M., Marleau, G.-D., Galicher, R., et al. 2014b, *A&A*, 567, L9
- Carbillot, M., Bendjoya, P., Abe, L., et al. 2011, *Experimental Astronomy*, 30, 39
- Chauvin, G., Desidera, S., Lagrange, A.-M., et al. 2017a, in SF2A-2017: Proceedings of the Annual meeting of the French Society of Astronomy and Astrophysics, ed. C. Reylé, P. Di Matteo, F. Herpin, E. Lagadec, A. Lançon, Z. Meliani, & F. Royer, 331–335
- Chauvin, G., Desidera, S., Lagrange, A.-M., et al. 2017b, *A&A*, 605, L9
- Chauvin, G., Lagrange, A.-M., Beust, H., et al. 2012, *A&A*, 542, A41
- Claudi, R. U., Turatto, M., Gratton, R. G., et al. 2008, in Society of Photo-Optical Instrumentation Engineers (SPIE) Conference Series, Vol. 7014, Society of Photo-Optical Instrumentation Engineers (SPIE) Conference Series, 3
- Dohlen, K., Langlois, M., Saisse, M., et al. 2008, in Society of Photo-Optical Instrumentation Engineers (SPIE) Conference Series, Vol. 7014, Society of Photo-Optical Instrumentation Engineers (SPIE) Conference Series, 3
- Galicher, R., Boccaletti, A., Mesa, D., et al. 2018, *A&A*, 615, A92
- Kiefer, F., Lecavelier des Etangs, A., Boissier, J., et al. 2014, *Nature*, 514, 462
- Lagrange, A.-M., Boccaletti, A., Milli, J., et al. 2012a, *A&A*, 542, A40
- Lagrange, A.-M., Bonnefoy, M., Chauvin, G., et al. 2010, *Science*, 329, 57
- Lagrange, A.-M., De Bondt, K., Meunier, N., et al. 2012b, *A&A*, 542, A18
- Lecavelier Des Etangs, A., Deleuil, M., Vidal-Madjar, A., et al. 1995, *A&A*, 299, 557
- Lecavelier des Etangs, A. & Vidal-Madjar, A. 2016, *A&A*, 588, A60
- Lecavelier Des Etangs, A., Vidal-Madjar, A., Burki, G., et al. 1997, *A&A*, 328, 311
- Maire, A.-L., Langlois, M., Dohlen, K., et al. 2016, in Proc. SPIE, Vol. 9908, Ground-based and Airborne Instrumentation for Astronomy VI, 990834
- Marois, C., Correia, C., Véran, J.-P., & Currie, T. 2014, in IAU Symposium, Vol. 299, IAU Symposium, ed. M. Booth, B. C. Matthews, & J. R. Graham, 48–49
- Marois, C., Lafrenière, D., Doyon, R., Macintosh, B., & Nadeau, D. 2006, *ApJ*, 641, 556
- Smith, B. A. & Terrile, R. J. 1984, *Science*, 226, 1421
- Snellen, I. A. G. & Brown, A. G. A. 2018, *Nature Astronomy*
- Sommer, R., Pueyo, L., & Larkin, J. 2012, *ApJ*, 755, L28
- Thébaud, P. & Beust, H. 2001, *A&A*, 376, 621
- van Leeuwen, F. 2007, *A&A*, 474, 653
- Wang, J. J., Graham, J. R., Pueyo, L., et al. 2016, *AJ*, 152, 97
- <sup>1</sup> Univ. Grenoble Alpes, CNRS, IPAG, F-38000 Grenoble, France
- <sup>2</sup> LESIA, Observatoire de Paris, PSL Research University, CNRS, Sorbonne Universits, UPMC Univ. Paris 06, Univ. Paris Diderot, Sorbonne Paris Cit, 5 place Jules Janssen, 92195 Meudon, France
- <sup>3</sup> Aix Marseille Université, CNRS, LAM (Laboratoire d’Astrophysique de Marseille) UMR 7326, 13388 Marseille, France
- <sup>4</sup> CRAL, UMR 5574, CNRS, Universit de Lyon, Ecole Normale Supérieure de Lyon, 46 Allée d’Italie, F-69364 Lyon Cedex 07, France
- <sup>5</sup> Unidad Mixta Internacional Franco-Chilena de Astronomía, CNRS/INSU UMI 3386 and Departamento de Astronomía, Universidad de Chile, Casilla 36-D, Santiago, Chile
- <sup>6</sup> INAF - Osservatorio Astronomico di Padova, Vicolo dell Osservatorio 5, 35122, Padova, Italy
- <sup>7</sup> ESO Alonso de Crdova 3107, Vitacura, Regin Metropolitana, Chili
- <sup>8</sup> Max Planck Institute for Astronomy, Königstuhl 17, D-69117 Heidelberg, Germany
- <sup>9</sup> Instiute for Particle Physics and Astrophysics, ETH Zurich, Wolfgang-Pauli-Strasse 27, 8093 Zurich, Switzerland
- <sup>10</sup> Department of Astronomy, University of Michigan, Ann Arbor, MI 48109, US
- <sup>11</sup> SUPA, Institute for Astronomy, The University of Edinburgh, Royal Observatory, Blackford Hill, Edinburgh, EH9 3HJ, UK
- <sup>12</sup> Department of Astrophysics, Denys Wilkinson Building, Keble Road, Oxford, OX1 3RH, UK
- <sup>13</sup> Department of Astronomy, Stockholm University, AlbaNova University Center, SE-10691, Stockholm, Sweden
- <sup>14</sup> INAF-Osservatorio Astrofisico di Catania, Via S. Sofia 78, I-95123 Catania, Italy
- <sup>15</sup> Geneva Observatory, University of Geneva, Chemin des Maillettes 51, 1290 Versoix, Switzerland
- <sup>16</sup> Núcleo de Astronoma, Facultad de Ingenierífa, Universidad Diego Portales, Av. Ejercito 441, Santiago, Chile
- <sup>17</sup> Anton Pannekoek Institute for Astronomy, Science Park 904, NL-1098 XH Amsterdam, The Netherlands
- <sup>18</sup> Université Cote d’Azur, OCA, CNRS, Lagrange, France
- <sup>19</sup> Leiden Observatory, Leiden University, PO Box 9513, 2300 RA Leiden, The Netherlands
- <sup>20</sup> INAF-Osservatorio Astronomico di Brera, Via E. Bianchi 46, I-23807 Merate, Italy
- <sup>21</sup> Exoplanets and Stellar Astrophysics Laboratory, Code 667, NASA Goddard Space Flight Center, Greenbelt MD, 20771, USA
- <sup>22</sup> Physikalisches Institut, Universitt Bern, Gesellschaftsstrasse 6, 3012, Bern, Switzerland
- <sup>23</sup> INAF - Osservatorio Astrofisico di Arcetri, Largo E. Fermi 5, I-50125 Firenze, Italy
- <sup>24</sup> INAF - Osservatorio Astronomico di Capodimonte, Salita Moiariello 16, 80131 Napoli, Italy
- <sup>25</sup> ONERA (Office National d’Etudes et de Recherches Aérospatiales), B.P.72, F-92322 Chatillon, France
- <sup>26</sup> European Southern Observatory (ESO), Karl-Schwarzschild-Str. 2, 85748 Garching, Germany
- <sup>27</sup> NOVA Optical Infrared Instrumentation Group, Oude Hoogeveensedijk 4, 7991 PD Dwingeloo, The Netherlands
- <sup>28</sup> Center for Theoretical Astrophysics and Cosmology, Inst. for Computational Science, University of Zürich, Winterthurerstrasse 190, CH-8057 Zürich, Switzerland

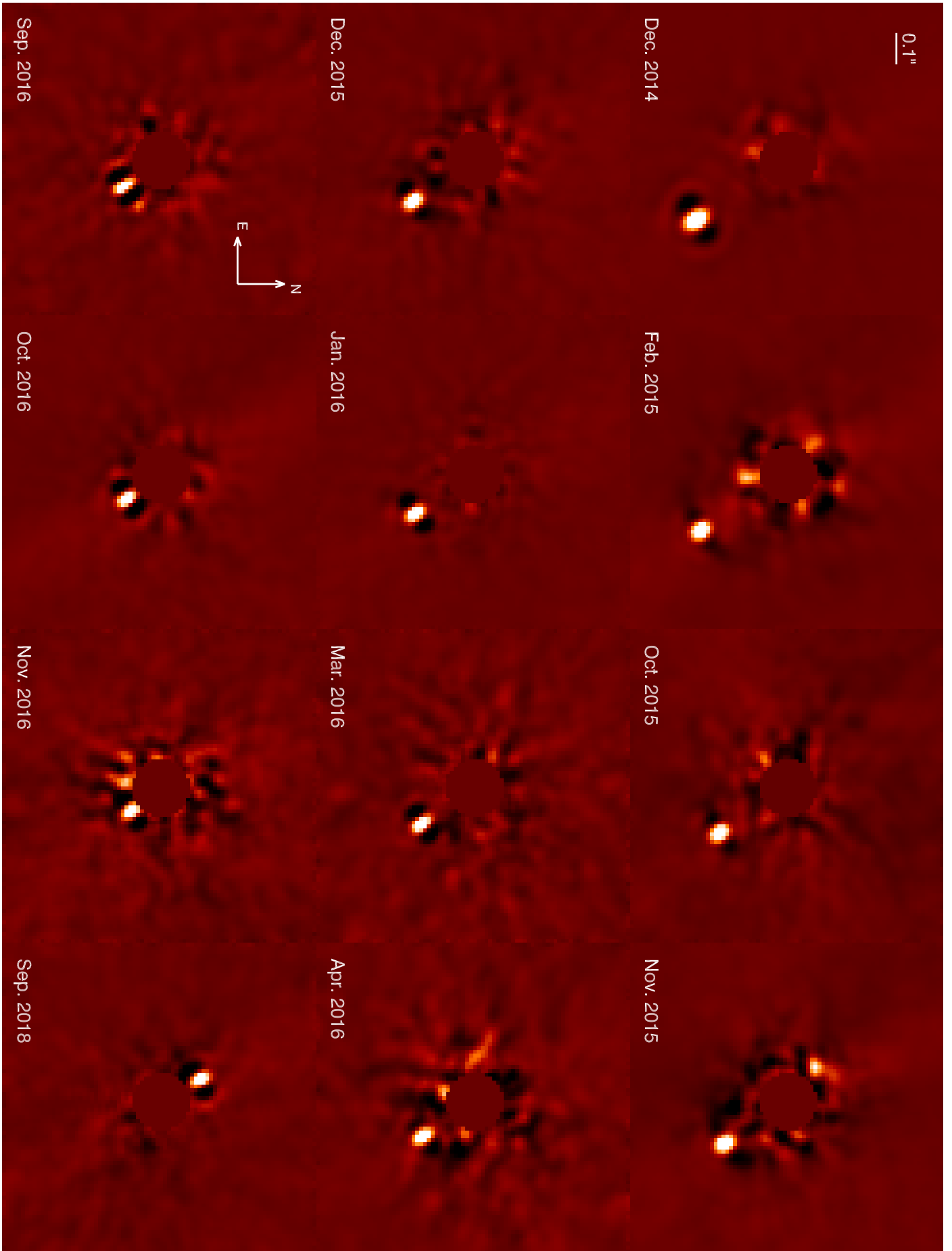


**Fig. 1.** Images of  $\beta$  Pictoris b with SPHERE IRDIS from December 2014 to September 2018. Each panel displays a FoV of  $1'' \times 1''$ . North is up and east is to the left. The intensity scale is adapted at each epoch according to the intensity peak of the planet.

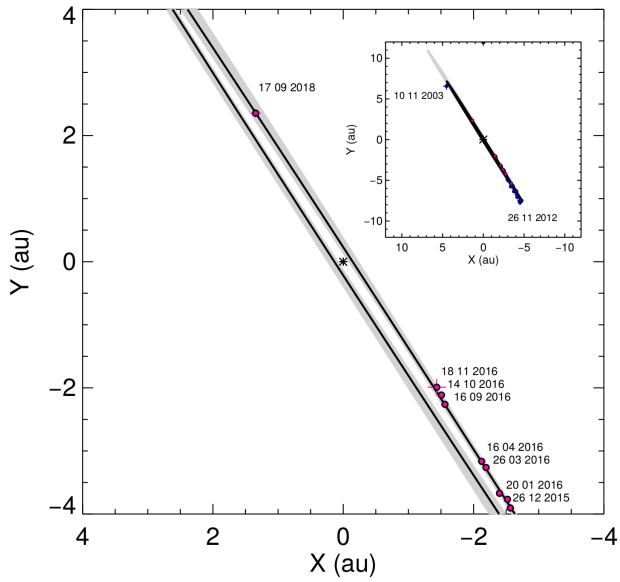


**Fig. 2.** NaCo (*blue*) and SPHERE (*magenta*) astrometric data points of  $\beta$  Pictoris b shown together with 200 probable solutions of the MCMC analysis (*gray*) and the best-fit Levenberg-Marquardt solution (*black*).



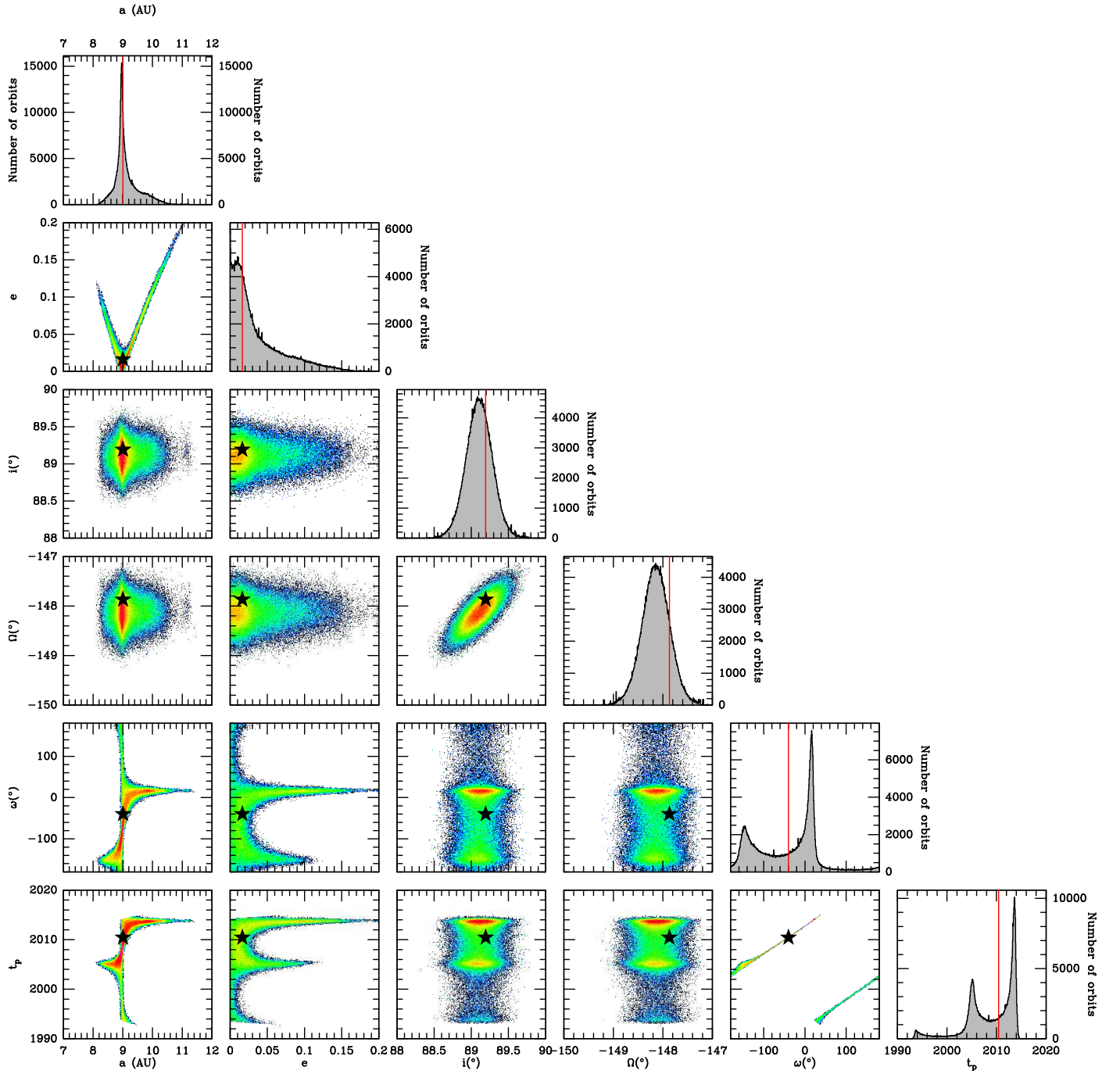


**Fig. 3.** Results of the MCMC fit of the NaCo + SPHERE astrometric data points. The star and the red dotted line correspond to the best-fit solution (best  $\chi^2$ ) obtained with a Levenberg-Marquardt fit.

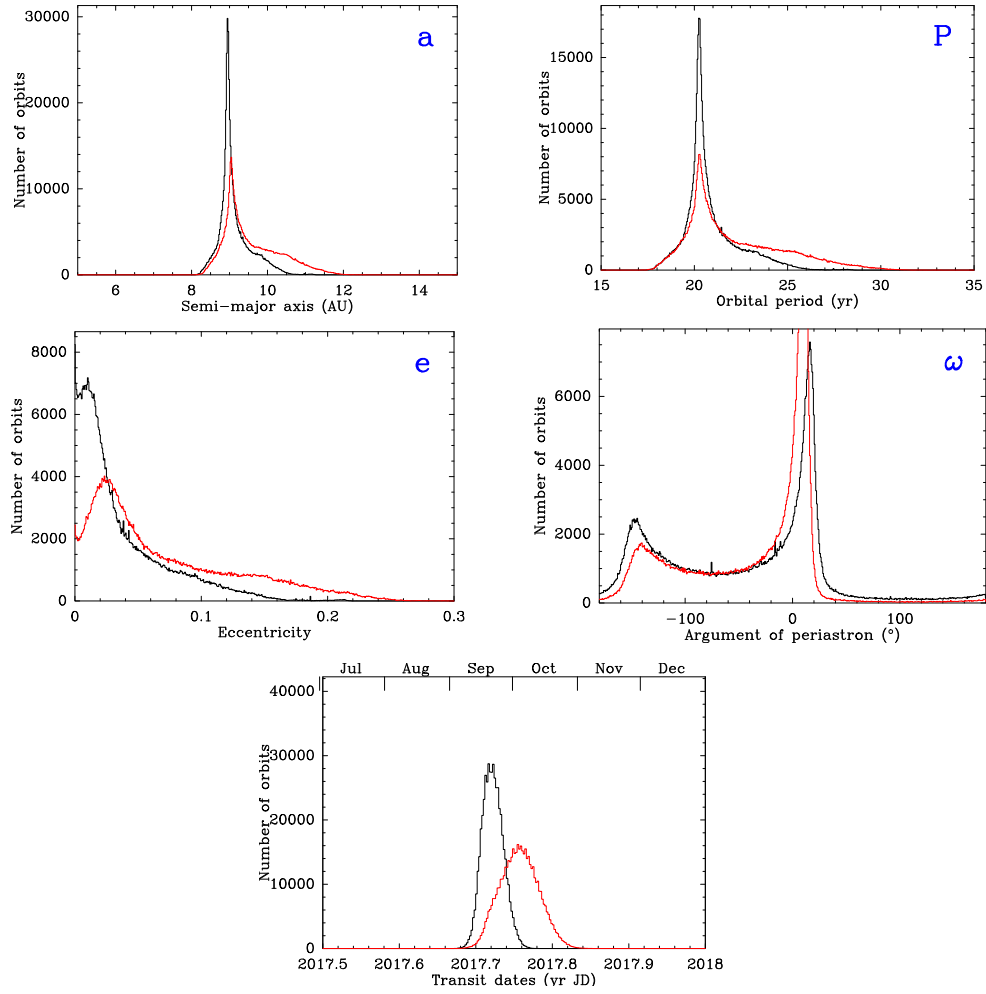


**Fig. 4.** Comparison between the orbital parameters obtained with (black) or without (red) the recovery point of September 2018.